VIII International Conference on Particle-Based Methods
PARTICLES 2023
U. Perego, M. Cremonesi, A. Franci (Eds)

BOTTOM BOUNDARY-FITTED FREE SURFACE FLOW SIMULATION WITH COORDINATE TRANSFORMATION USING SPH(2)

S. FUJIOKA[1], K. TSUJI[2], N. MITSUME[3] AND M. ASAI[4]

[1] Department of Civil Engineering, Graduate School of Engineering, Kyushu University
744 Motooka, Nishi-ku, Fukuoka, Fukuoka 819-0395, Japan
e-mail: s-fujioka@doc.kyushu-u.ac.jp

[2] Dr. Eng., Department of Civil Engineering, Graduate School of Engineering,
Tohoku University 6-6-06 Aramakiaoba, Aoba-ku, Sendai, Miyagi, 980-8579, Japan
e-mail: kumpei.tsuji.e1@tohoku.ac.jp

[3] Dr. Eng., Faculty of Engineering, Information and Systems, Tsukuba University
1-1-1 Tennodai, Tsukuba, Ibaraki, 305-8577, Japan
e-mail: mitsume@kz.tsukuba.ac.jp

[4] Department of Civil Engineering, Graduate School of Engineering, Kyushu University
744 Motooka, Nishi-ku, Fukuoka, Fukuoka 819-0395, Japan
e-mail: asai@doc.kyushu-u.ac.jp

Abstract: Particle methods such as the SPH and MPS methods have problems because it is difficult to treat curved bottom surfaces such as seabed surfaces accurately. In this study, regarding this problem, the curved bottom surfaces' treatments have been improved using a coordinate transformation using the high-order second derivative model called SPH(2). Although the theory for the coordinate transformation was established in the MPS method, its accuracy did not give the desired accuracy because of the numerical errors of the second derivative models. Therefore, the numerical errors in these coordinate transformations were overcome by applying the second derivative model of SPH(2) to the coordinate transformation formulas. The superiority and validity of the proposed coordinate transformation using SPH(2) are demonstrated through validation examples such as the hydrostatic pressure and dam-break problems.

Keywords. SPH, Coordinate Transformation, Derivative Model, Dam-break Problem

1 INTRODUCTION

The SPH (Smoothed Particle Hydrodynamics) method [1, 2] is one of the several Lagrangian mesh-free particle methods, and it is widely applied to fluid dynamics problems such as landslide simulation and tsunami simulation. In the SPH method, particles move with the flow, and their arrangement is disordered. Where the general SPH approximation using particles [1, 2] to approximate the value of functions and their derivatives have the

characteristic that accuracy is guaranteed only for regular particle arrangements. Therefore, it is necessary for numerical analysis accuracy to correct approximations depending on particle arrangements. Regarding this problem, we proposed the high-order second derivative model called SPH(2) [3]. SPH(2) satisfies up to the 2nd-order terms of the Taylor expansion and can evaluate the gradient besides the second derivatives. In addition, SPH(2) can be applied to analysis involving anisotropic diffusions [4] and coordinate transformation [5] because SPH(2) can evaluate each of the second derivatives.

Furthermore, while the SPH method has been applied to disaster simulation, the treatment of boundaries, including curved surfaces such as seabed, is an issue to improve the accuracy. FWGPs(Fixed Wall Ghost Particles) [6] is one of the most common ways to approach wall boundaries. However, this method is characterized by arranging wall particles in a grid-like fashion, which leads to the formation of steps when representing curved or sloped surfaces. Regarding this problem, Matsumoto et al. proposed a bottom boundary-fitted MPS method [5] with coordinate transformation and validated this method's accuracy. However, its accuracy did not give the desired accuracy because of the numerical errors of the second derivative models. In this paper, the numerical errors in these coordinate transformations are overcome by applying the second derivative model of SPH(2) to the coordinate transformation formulas. The superiority and validity of the proposed coordinate transformation using SPH(2) are demonstrated through validation examples such as the hydrostatic pressure problem and dam-break problem.

2 SPH METHOD FORMULATION

2.1 Governing equations

In this study, we use the Incompressible SPH method for the incompressible flows. Therefore, the governing equations are the following continuity and Navier–Stokes equations:

$$\nabla \cdot \boldsymbol{v} = 0, \tag{1}$$

$$\frac{D\boldsymbol{v}}{Dt} = -\frac{1}{\rho}\nabla p + \nu\nabla^2\boldsymbol{v} + \boldsymbol{f}, \tag{2}$$

where $\boldsymbol{v}$ denotes velosity, ρ denotes fluid density, p denotes pressure, nu denotes kinematic viscosity, $\boldsymbol{f}$ denotes external force.

2.2 The SPH approximations

The SPH method is a space integration method that smoothly approximates the value of functions and their derivatives by integrating the contribution of the neighbor particles, varying its influence according to a weight function w, which is chosen from a wide range of possibilities. In this study, we used the cubic spline function. Then, one can approximate the value of a generic function for a given particle and its derivatives as follows:

$$\langle\phi\rangle_i := \sum_{j\in\mathbb{S}_i} \frac{m_j}{\rho_j}\phi_j w_{ij}, \tag{3}$$

$$\langle \nabla \phi \rangle_i := \sum_{j \in \mathbb{S}_i} \frac{m_j}{\rho_j} \phi_{ij} \nabla w_{ij}, \tag{4}$$

$$\langle \nabla \cdot \boldsymbol{\phi} \rangle_i := \sum_{j \in \mathbb{S}_i} \frac{m_j}{\rho_j} \boldsymbol{\phi}_{ij} \nabla \cdot w_{ij}, \tag{5}$$

$$\langle \nabla^2 \phi \rangle_i := 2 \sum_{j \in \mathbb{S}_i} \frac{m_j}{\rho_j} \phi_{ij} \frac{\boldsymbol{r}_{ij} \cdot \nabla w_{ij}}{|\boldsymbol{r}_{ij}|}, \tag{6}$$

$$\mathbb{S}_i := \{ j = 1, 2, \cdots, N_{\mathrm{SPH}} \mid \quad |\boldsymbol{r}_{ij}| < 2h \wedge \boldsymbol{r}_j \in \Omega \}, \tag{7}$$

where the subscripted indices i and j denote the target and neighboring particles, respectively, m denotes mass, $\boldsymbol{r}$ denotes position vector ($\boldsymbol{r}_{ij} := \boldsymbol{r}_j - \boldsymbol{r}_i$), ϕ and $\boldsymbol{\phi}$ denote scalar and vector function ($\phi_i := \phi(\boldsymbol{r}_i, t)$, $\boldsymbol{\phi}_i := \boldsymbol{\phi}(\boldsymbol{r}_i, t)$, $\phi_{ij} := \phi_j - \phi_i$, $\boldsymbol{\phi}_{ij} := \boldsymbol{\phi}_j - \boldsymbol{\phi}_i$), respectively, and symbol $\langle \cdot \rangle$ denote the application of the SPH approximation.

2.3 Time integration based on the projection method

First, the contribution of the viscous term and the external forces of Eq. (2) results in a predicted velocity field calculated implicitly as follows:

$$\boldsymbol{v}^* = \boldsymbol{v}^N + \Delta t (\nu \nabla^2 \boldsymbol{v}^N + \boldsymbol{f}). \tag{8}$$

Then, the pressure is calculated from a pressure Poisson equation:

$$\nabla^2 p^{N+1} = -\frac{\rho}{\Delta t} \nabla \cdot \boldsymbol{v}^*. \tag{9}$$

Finally, adding the contribution of the pressure field, we implicitly calculate the updated velocity field as follows:

$$\boldsymbol{v}^{N+1} = \boldsymbol{v}^* + \Delta t \left(-\frac{\nabla p^{N+1}}{\rho} \right), \tag{10}$$

where N and $N+1$ refer to the current and next iterations, the superscript $*$ denotes the predictor step. Eqs. (8) and (9) are the predictor and corrector steps, respectively.

In this study, the following equation is solved by adding a term to the pressure Poisson equation as in [7]:

$$\langle \nabla^2 p^{N+1} \rangle_i = -\frac{\rho}{\Delta t} \langle \nabla \cdot \boldsymbol{v}^* \rangle_i + \alpha \frac{\rho - \langle \rho^N \rangle_i}{\Delta t^2}, \tag{11}$$

where $\alpha (\ll 1)$ is the coefficient to keep the total fluid volume called the relaxation coefficient.

3 BOTTOM BOUNDARY-FITTED PARTICLE METHOD

In this section, we summarized the bottom boundary-fitted particle method using coordinate transformation [5] and explained the SPH approximation models used in this study.

3.1 Coordinate transformation

In this study, we used the coordinate transformation depending on the bottom height shown in Fig. 1. This makes it possible to represent curved surfaces and slopes with simple planes.

When the height of the bottom boundary from the dashed line in Fig. 1 is $h(x)$, the coordinate transformation is defined as follows:

$$\xi = x, \tag{12}$$
$$\zeta = y - h(x). \tag{13}$$

The Jacobi matrix $\boldsymbol{J}$ of this coordinate transformation is expressed as follows:

$$\boldsymbol{J} = \begin{bmatrix} \dfrac{\partial \xi}{\partial x} & \dfrac{\partial \zeta}{\partial x} \\ \dfrac{\partial \xi}{\partial y} & \dfrac{\partial \zeta}{\partial y} \end{bmatrix} = \begin{bmatrix} 1 & \dfrac{dh}{dx} \\ 0 & 1 \end{bmatrix} \tag{14}$$

Therefore, gradient and Laplacian in $x-y$ coordinate are calculated using $\xi-\zeta$ coordinate as follows:

$$\nabla\phi = \boldsymbol{J}\widehat{\nabla}\phi \quad ; \widehat{\nabla} = \begin{bmatrix} \dfrac{\partial}{\partial \xi} & \dfrac{\partial}{\partial \zeta} \end{bmatrix}^T, \tag{15}$$

$$\nabla^2\phi = \boldsymbol{J}\widehat{\nabla} \cdot \boldsymbol{J}\widehat{\nabla}\phi = \boldsymbol{c}_{\mathrm{trans}} \cdot \widehat{\boldsymbol{D}}\phi, \tag{16}$$

$$\boldsymbol{c}_{\mathrm{trans}} := \begin{bmatrix} 0 & -\dfrac{d^2h}{dx^2} & 1 & -2\dfrac{dh}{dx} & 1 + \left(\dfrac{dh}{dx}\right)^2 \end{bmatrix}^T, \tag{17}$$

$$\boldsymbol{D} := \begin{bmatrix} \dfrac{\partial}{\partial \xi} & \dfrac{\partial}{\partial \zeta} & \dfrac{\partial^2}{\partial \xi^2} & \dfrac{\partial^2}{\partial \xi \partial \zeta} & \dfrac{\partial^2}{\partial \zeta^2} \end{bmatrix}^T. \tag{18}$$

Using the above derivatives, the governing equations in $x-y$ coordinate are written as follows:

$$\frac{D\boldsymbol{v}}{Dt} = -\frac{1}{\rho}\boldsymbol{J}\widehat{\nabla}p + \nu \boldsymbol{c}_{\mathrm{trans}} \cdot \widehat{\boldsymbol{D}}\boldsymbol{v} + \boldsymbol{f}, \tag{19}$$

$$\boldsymbol{J}\widehat{\nabla} \cdot \boldsymbol{v} = 0. \tag{20}$$

From the above, by solving the above governing equations in $\xi-\zeta$ coordinate, the motion of the fluid in $x-y$ coordinate can be analyzed. The bottom boundary-fitted particle method has $\det \boldsymbol{J} = 1$, so the volume does not change.

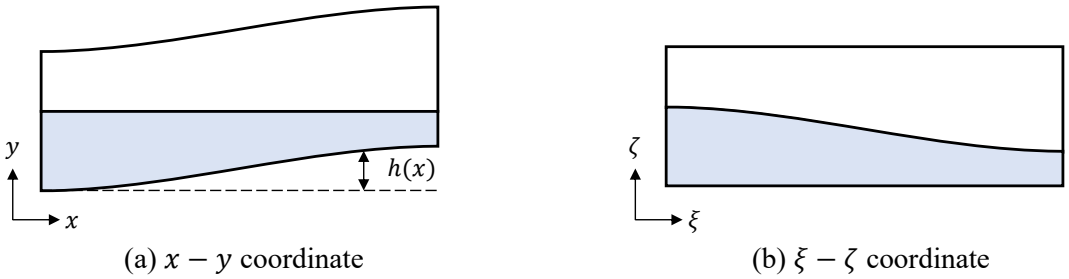

(a) $x-y$ coordinate (b) $\xi-\zeta$ coordinate

Figure 1: Schematic view of coordinate transformation

Table 1: Case names for fluid analysis

case names	velocity divergence	pressure gradient	second derivatives
0th–0th	1st-order model[8]	Monaghan[9]	Español and Revenga[10]
2nd–1st	1st-order model	1st-order model	SPH(2)

3.2 SPH particle approximation models

As shown in Eq. 18, the numerical analysis with coordinate transformation requires the SPH approximation that can evaluate the second derivatives. However, the Laplacian model can only evaluate the Laplacian, not the individual second derivatives, as shown in Eq. (6). Thus, in this study, the SPH approximation different from the general ones shown in Table 1 is used for the analysis.

The model used for velocity divergence is expressed as follows:

$$\langle \nabla \phi \rangle_i^{1\mathrm{st}} := \sum_{j \in \mathbb{S}_i} \frac{m_j}{\rho_j} \phi_{ij} \widetilde{\nabla} w_{ij} \qquad ; \widetilde{\nabla} w_{ij} := \left[\sum_{j \in \mathbb{S}_i} \frac{m_j}{\rho_j} (\nabla w_{ij} \otimes \boldsymbol{r}_{ij}) \right]^{-1} \nabla w_{ij}. \tag{21}$$

This model is a high-order gradient model widely used in the SPH method. It is derived to satisfy the 1st-order terms of the Taylor expansion.

The model used for pressure gradient in the 0th–0th case is expressed as follows:

$$\langle \nabla p \rangle_i := \rho_i \sum_{j \in \mathbb{S}_i} m_j \left(\frac{p_j}{\rho_j^2} + \frac{p_i}{\rho_i^2} \right) \nabla w_{ij}. \tag{22}$$

This model is used to calculate pressure gradient in the general SPH method because of its high numerical stability..

The model used for second derivatives in the 0th–0th case is expressed as follows:

$$\left\langle \frac{\partial^2 \phi}{\partial r^I \partial r^J} \right\rangle_i := \sum_{j \in \mathbb{S}_i} \frac{m_j}{\rho_j} \phi_{ij} \frac{\boldsymbol{r}_{ij} \cdot \nabla w_{ij}}{|\boldsymbol{r}_{ij}|^2} \left(\frac{4 r_{ij}^I r_{ij}^J}{|\boldsymbol{r}_{ij}|^2} - \delta^{IJ} \right). \tag{23}$$

This model is derived assuming unity conditions and regular particle arrangements. Since these are the same conditions as the general Laplacian model, the accuracy of Eq. (6) and Eq. (23) is equivalent.

SPH(2), proposed by us, used for second derivatives in 2nd–1st case is expressed as follows:

$$\left[\left\langle\frac{\partial^2\phi}{\partial x^2}\right\rangle_i \quad \left\langle\frac{\partial^2\phi}{\partial y^2}\right\rangle_i \quad 2\left\langle\frac{\partial^2\phi}{\partial x\partial y}\right\rangle_i\right]^T := 2\left[\mathbf{M}_i\right]\sum_{j\in\mathbb{S}_i}\frac{m_j}{\rho_j}F_{ij}\left[\mathbf{q}_i\right]\left(\phi_{ij}-\boldsymbol{r}_{ij}\cdot\langle\nabla\phi\rangle_i^{\mathrm{1st}}\right), \tag{24}$$

$$\left[\mathbf{M}_i\right] := \sum_{j\in\mathbb{S}_i}\frac{m_j}{\rho_j}F_{ij}\left[\mathbf{q}_i\right]\left[\mathbf{p}_i\right]^T \quad ; F_{ij} := \frac{\boldsymbol{r}_{ij}\cdot\widetilde{\nabla}w_{ij}}{|\boldsymbol{r}_{ij}|^4}, \tag{25}$$

$$\left[\mathbf{q}_i\right] := \begin{bmatrix}x_{ij}^2 & y_{ij}^2 & x_{ij}y_{ij}\end{bmatrix}^T, \tag{26}$$

$$\left[\mathbf{p}_i\right] := \begin{bmatrix}A(x,x) & A(y,y) & A(x,y)\end{bmatrix}^T \quad ; A(a,b) = a_{ij}b_{ij} - \boldsymbol{r}_{ij}\cdot\sum_{k\in\mathbb{S}_i}\frac{m_k}{\rho_k}a_{ik}b_{ik}\widetilde{\nabla}w_{ik}. \tag{27}$$

This model is derived to satisfy the 2nd-order terms of the Taylor expansion.

In the numerical analysis with coordinate transformation, the SPH approximations shown in this section are performed in $\xi-\zeta$ coordinate, and the Jacobi matrix $\boldsymbol{J}$ is used for correction to $x-y$ coordinate.

4 STABILIZED METHOD

Numerical instability due to particle agglomeration, disorder, and missing particles is likely to occur in problems with free surfaces. Even if a high-order derivative model is used, the disorder of the particle arrangement leads to a decrease in accuracy. This study corrected the particle arrangement to a more regular arrangement by applying PST (Particle Shifting Technique). This particle rearrangement technique is often used in recent particle methods. Specifically, OPS (Optimized Particle Shifting) [11], DS (Dynamic Stabilizer) [12]. In addition, the XSPH method [13] is introduced for free surface particles to smooth out the velocity at the free surface. The proposed method applies PST to the particle configuration in $\xi-\zeta$ coordinate to evaluate the derivative of $x-y$ coordinate in $\xi-\zeta$ coordinate.

In this study, the shifting parameter for OPS is set to 0.2, the ratio of the time step to the Courant number for DS to 0.2, and the smoothing parameter for the XSPH method to 1.0×10^{-2}.

5 NUMERICAL RESULTS

In this section, we validate the accuracy of fluid analysis with coordinate transformation using SPH(2). Validation is performed through the hydrostatic pressure problem with the coordinate transformation applied to the whole space and through a dam-break problem with the coordinate transformation applied to a part of the space.

5.1 Hydrostatic pressure problem

The 2-dimensional hydrostatic pressure problem in a tank with a wavy bottom is calculated. The horizontal width of the tank is 50 cm, and the bottom is wavy, as indicated by the sin function.

Table 2: Computational conditions of hydrostatic pressure problem

Time step width	Δt	1.0×10^{-4}	[s]
Initial particle spacing	d_0	0.5	[cm]
Relaxation coefficient	α	1.0×10^{-2}	[-]
Fluid density	ρ	1.0	[g/cm^3]
Kinematic viscosity	ν	9.8×10^{-3}	[cm^2/s]
Gravitational acceleration	g	9.8×10^2	[cm/s^2]

The coordinate transformation for this problem is expressed as follows:

$$\xi = x, \tag{28}$$

$$\zeta = y + R_{\sin} \sin\left(\frac{2\pi x}{50}\right), \tag{29}$$

where $R_{\sin}$ denotes an arbitrary constant that defines the curvature of the bottom surface. The exact solution for the pressure in this validation is expressed as follows:

$$p^{\text{exact}}(y) = \rho g(H - y), \tag{30}$$

where g denotes the magnitude of gravitational acceleration and H denotes the depth from the water surface. $y = 0$ is the position indicated by the dashed line in Fig. 1, and the water surface is set 50 cm above that line. To validate during hydrostatic pressure, the numerical results are used for the real-time $t = 10$ s for validation.

The computational conditions are shown in Table 2. The wall boundary approach in this analysis uses the FWGPs(Fixed Wall Ghost Particles), and the velocity of the wall particles is given by the non-slip condition with $|\boldsymbol{v}| = 0$. For the hydrostatic pressure problem, analyses are performed for 0th–0th case and 2nd–1st case shown in Section 3.

Fig. 2 cm shows the pressure field for each case for $R_{\sin} = 2$. In the 0th–0th case, the pressure field is disturbed near the bottom boundary. In the 2nd–1st case, the disturbance is improved, resulting in a smooth pressure field.

Figs. 3 and 4 show the pressure field for each case for $R_{\sin} = 6$ cm and $R_{\sin} = 10$ cm, respectively. In the 0th–0th case, the pressure field is disturbed near the bottom boundary as for $R_{\sin} = 2$ cm. Furthermore, although 0th–0th case for$R_{\sin} = 10$ cm is possible to analyze up to a real-time $t = 10$ s, the pressure field is unphysical as shown in Fig. 4(a). On the other hand, in case 2nd–1st, a smooth pressure distribution is obtained regardless of the value of $R_{\sin}$.

Fig. 5 compares pressure distribution by numerical analysis and exact solution. This result shows that the accuracy for the 2nd–1st case is higher than that for the 0th–0th case and that reasonable results are obtained. However, even when the analysis is performed for the 2nd–1st case, the solution diverged for $R_{\sin} > 14$ cm. Stable analysis at $R_{\sin} > 14$ cm is essential for real-world applications. Therefore, we will solve this problem by improving the boundary conditions in the future.

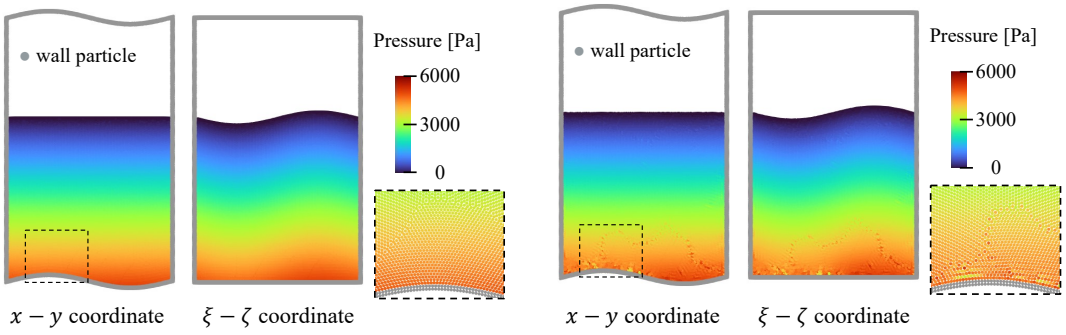

(a) 0th−0th (b) 2nd−1st

Figure 2: Pressure field for $R_{\sin} = 2$

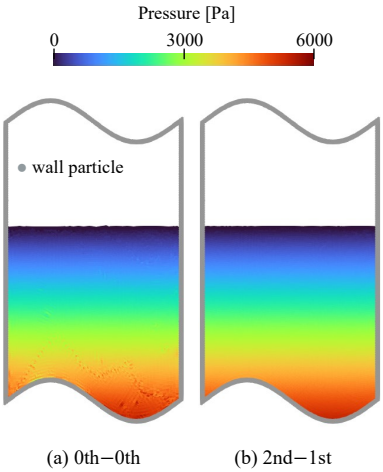

(a) 0th−0th (b) 2nd−1st

Figure 3: Pressure field for $R_{\sin} = 6$

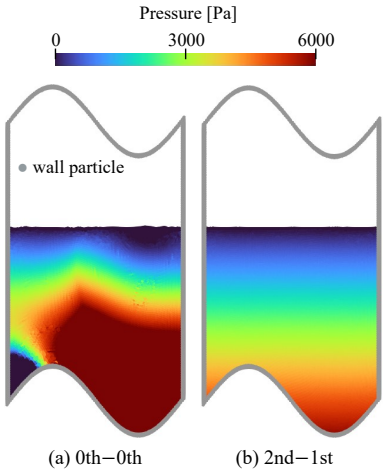

(a) 0th−0th (b) 2nd−1st

Figure 4: Pressure field for $R_{\sin} = 10$

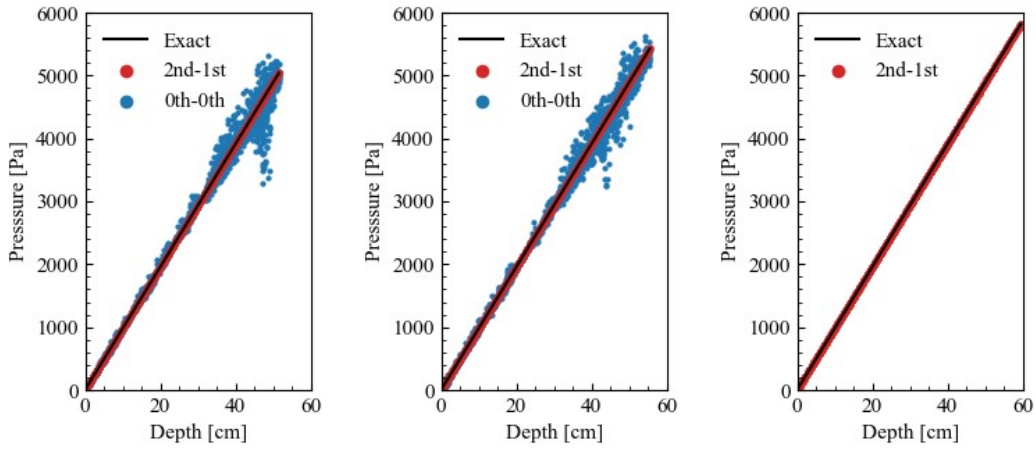

(b) $R_{\sin} = 2$ (b) $R_{\sin} = 6$ (b) $R_{\sin} = 10$

Figure 5: Pressure distribution

5.2 Dam-break problem

A dam-break problem that results in flow over a triangular bottom sill is calculated. The initial conditions are defined as depicted in Fig. 6. This validation compares the experiment [14] with the numerical analysis results. In the experiment, water levels were measured sequentially for up to 45 seconds in real-time at three water level gauges: G1, G2, and G3. The x-coordinate values of G1, G2, and G3 are 393.5 cm, 492.5 cm, and 557.5 cm, respectively.

The computational conditions are shown in Table 3. The wall boundary approach in this analysis is the same as for the hydrostatic pressure problem.

Figs. 9 and 10 show the numerical analysis results around the gauges for 0th–0th and 2nd–1st cases, respectively. In the area to the right of a triangular bottom sill, the results for 2nd–1st case A are generally consistent with the water surface shape in the experiment. However, the two cases do not differ significantly in the area to the left of the triangular bottom sill. They are not consistent with the water surface shape in the experiment. This is thought to be due to analysis of a 3-dimensional experiment in 2-dimensions.

Figs. 9 and 10 show the time trends of water level for 0th–0th and 2nd–1st cases, respectively. The results of point G1 show that the waves for the 0th–0th case decay significantly, whereas the water level trend for the 2nd–1st case generally agrees with the experiment. The results of points G2 and G3 show that the final water level for the 0th-0th case is closer to the experiment than for the 2nd–1st case. However, time trends of water level are consistent for the 2nd–1st and are constant after about 20 seconds for the 0th–0th. Therefore, we consider that the results of the 2nd–1st analysis are valid and that the errors with the experiment are due to the number of dimensions, particles, and so on. Furthermore, since the difference in results for different particle spacing is smaller for the 2nd–1st than for the 0th–0th, the number of particles required to guarantee accuracy is expected to decrease.

Table 3: Computational conditions of hydrostatic problem

Time step width	Δt	$d_0/0.4 \times 10^{-4}$	[s]
Initial particle spacing	d_0	0.4, 0.2	[cm]
Relaxation coefficient	α	$\Delta t/2 \times 10^2$	[-]
Fluid density	ρ	1.0	[g/cm^3]
Kinematic viscosity	ν	9.8×10^{-3}	[cm^2/s]
Gravitational acceleration	g	9.8×10^2	[cm/s^2]

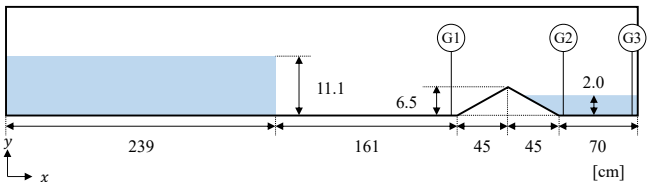

Figure 6: Schematic diagram of dam-break problem

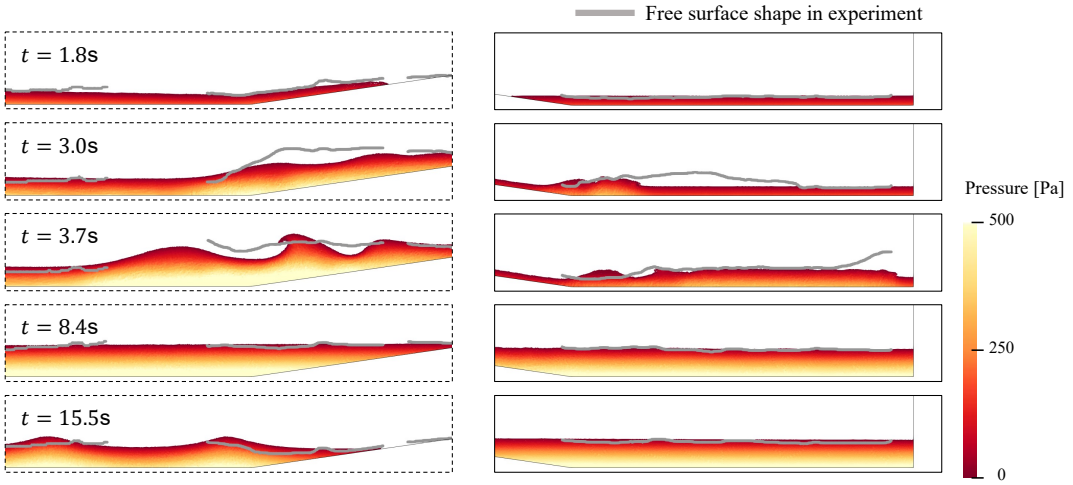

Figure 7: Comparison of free surface shape with experiment for 0th–0th case

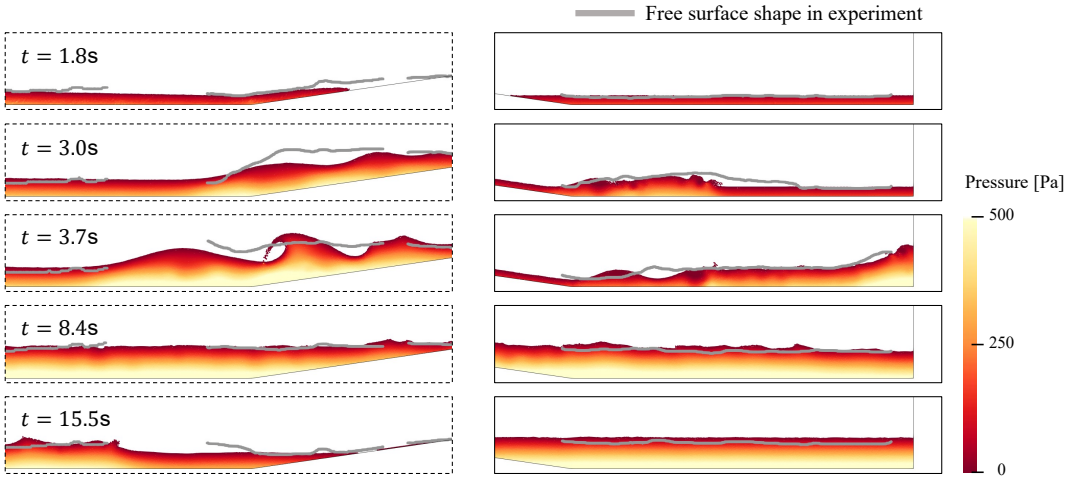

Figure 8: Comparison of free surface shape with experiment for 2nd–1st case

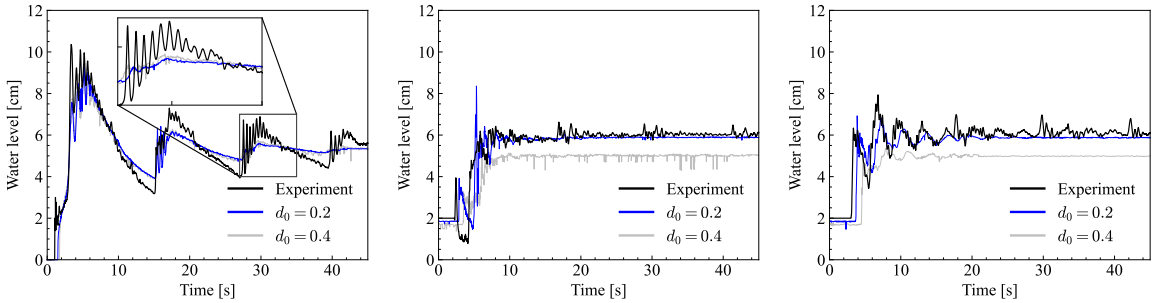

(a) G1 (b) G2 (c) G3

Figure 9: Time trends of water level for 0th–0th case

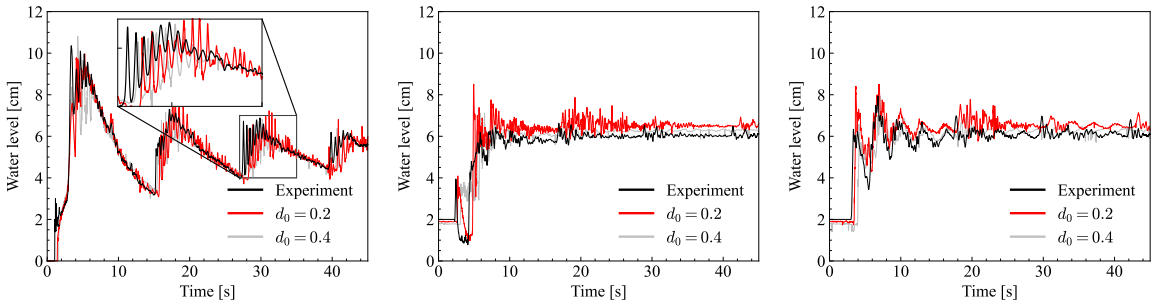

(a) G1 (b) G2 (c) G3

Figure 10: Time trends of water level for 2nd–1st case

6 CONCLUSIONS

In this paper, we applied SPH(2), a high-order 2nd-order derivative model, to a bottom boundary-fitted particle method with coordinate transformation. This method improves the accuracy of the approximation due to the disorder of the particle configuration and improves the accuracy of the representation of curved bottom surfaces. In validating the hydrostatic pressure problem, the disturbance of the pressure field for the 0th-0th case was eliminated for the 2nd-1st case using SPH(2), and the results generally agreed with the exact solution regardless of the curvature. For the dam-break problem, the wave attenuation for the 0th-0th case was eliminated for the 2nd-1st case, and the time trends of the water levels and bathymetry were in good agreement with experimental data. It was also confirmed that the analysis can be performed at coarse resolution without significantly reducing accuracy. However, validating the hydrostatic pressure problem confirmed that the calculation breaks down when the curvature exceeds a certain level. It is necessary to handle more complicated boundaries for application to disaster simulations. In addition, the lack of resolution and the fact that the analysis is conducted under 2-dimensional conditions are considered to be the cause of the error compared to the experiment.

As for future work, we aim to overcome this problem by reviewing the handling of boundary conditions. In addition, we plan to introduce a coordinate transformation to σ-coordinate [15], which divides the coordinates in the vertical direction, to reduce the computational cost, which is one of the significant issues in the particle method.

REFERENCES

[1] Lucy, L. B. A numerical approach to the testing of the fission hypothesis. *Astron. J.* (1977) **82**:1013–1024.

[2] Gingold, R.A. and Monaghan, J.J. Smoothed particle hydrodynamics: theory and application to non-spherical stars. *Mon. Not. R. Astron. Soc.* (1977) **181**:375–389.

[3] Asai, M., Fujioka, S., Saeki, Y., Morikawa, D. and Tsuji, K. A class of second derivatives in the Smoothed Particle Hydrodynamics with 2nd-order accuracy and its appli-

cation to incompressible flow simulations. *Comput. Methods Appl. Mech. Eng.* (2023) **415**:116203.

[4] Lian, Y., Bui, H. H., Nguyen, G. D., Tran, H. T. and Haque, A. A general SPH framework for transient seepage flows through unsaturated porous media considering anisotropic diffusion. *Comput. Methods Appl. Mech. Eng.* (2021) **387**:114169.

[5] Matsumoto, K. Imoto, Y. Asai, M. and Mitsume, N. Development of bottom boundary-fitted MPS method. *Transactions of JSCES* (2021) **2021**:20210017. (Japanese)

[6] Morikawa, D., Asai, M., Idris, N., Imoto, Y. and Isshiki, M. Improvements in highly viscous fluid simulation using a fully implicit SPH method. *Comput. Part. Mech.* (2019) **6**:529—544.

[7] Asai, M., Aly, A. M., Sonoda, Y. and Sakai, Y. A stabilized incompressible SPH method by relaxing the density invariance condition. *J. Appl. Math.* (2012) **2012**.

[8] Bonet, J. and Lok, T. S. Variational and momentum preservation aspects of smooth particle hydrodynamic formulations. *Comput. Methods Appl. Mech. Eng.* (1999) **180**(1-2):97–115.

[9] Monaghan, J. J. Smoothed particle hydrodynamics. *Rev. Astron. Astrophys.* (1992) **30**(1):543–574.

[10] Español, P. and Revenga, M. Smoothed dissipative particle dynamics. *Phys. Rev. E* (2003) **67**:026705.

[11] Khayyer, A., Gotoh, H. and Shimizu, Y. Comparative study on accuracy and conservation properties of two particle regularization schemes and proposal of an optimized particle shifting scheme in ISPH context. *J. Comput. Phys.* (2017) **332**:236–256.

[12] Tsuruta, N., Khayyer, A. and Gotoh, H. A short note on dynamic stabilization of moving particle semi-implicit method. *Comput. Fluids* (2013) **82**:158–164.

[13] Monaghan, J. J. Simulating free surface flows with SPH. *J. Comput. Phys.* (1994) **110**(2):399–406.

[14] Soares-Frazão, S. Experiments of dam-break wave over a triangular bottom sill. *J. Hydraul. Res.* (2007) **45**(sip1):19–26.

[15] Phillips, N. A. A coordinate system having some special advantages for numerical forecasting. *J. Meteor.* (1957) **14**:184–185.